ELSEVIER

Thermochimica Acta 300 (1997) 43–65

thermochimica acta

The heat capacity of polymers[1]

B. Wunderlich[2*]

Department of Chemistry, The University of Tennessee, Knoxville, TN 37996-1600, USA

Received 13 August 1996; accepted 15 November 1996

Abstract

The long path to an understanding of heat capacity is traced from isothermal and adiabatic calorimetries to the most recent three methods of isoperibol, scanning, and temperature-modulated calorimetry (TMDSC). These latter three methods are: the traditional method of *scanning thermal analysis*; the *quasi-isothermal method* of finding the maximum amplitude of the periodic heat flow in response to a temperature modulation at a constant base temperature; and the *pseudo-isothermal analysis* of a temperature-modulated scanning experiment by subtracting the effect due to the underlying constant heating rate. In parallel, the development of the knowledge about phases and molecules is traced from its beginning to present-day *nanophases* and *macromolecules*. © 1997 Elsevier Science B.V.

Keywords: Calorimetry; Heat capacity; Macromolecule; Phase; Thermal analysis; Transition

1. Introduction

Heat capacity and *polymers* are two subjects that are somewhat neglected when compared to the parallel-fields structure and small molecules. The understanding of the phenomenon *heat* was slow in developing over the last 300 years, and polymers – better known as *flexible macromolecules*[3] – have been solidly established only since 1920 through the work of Staudinger [1]. In this paper, an attempt is made to give an overview of the roots of measurement, an understanding of heat capacity as well as the development of knowledge about polymers and phases, ending in the exciting new methods of isoperibol, temperature-modulated differential scanning calorimetry (TMDSC), developed over the last five years, and new and promising *polymeric mesophases* that are not fully explored, but extend many of our well-established, classical ideas about the thermodynamics of phases and phase transitions.

2. Historical notes

After considerable discussion by many Greek philosophers, Plato and Aristotle, in the 4th century BC,

*Corresponding author. Fax: 00 1 (423) 974 3419.

[1]The submitted manuscript has been authored by a contractor of the U.S. Government under the contract No. DE-AC05-96OR22464. Accordingly, the U.S. Government retains a non-exclusive, royalty-free licence to publish, or reproduce the published form of this contribution, or allow others to do so, for U.S. Government purposes.

[2]Chemistry and Analytical Sciences Division, Oak Ridge National Laboratory, Oak Ridge, TN 37831-6197, USA.

[3]A macromolecule has been defined by Staudinger as a molecule with more than 1000 atoms or with a molar mass larger than 10 000 Da. To be flexible, some or all of the bonds that make up the structure of the macromolecule must be covalent, with a cylindrically symmetric bond, such as the hydrid orbitals types sp^2 or sp^3. This molecular structure permits internal rotation and leads to multiple conformational isomers in the condensed mobiles states (liquid or melt and mesophases).

PII S0040-6031(96)03126-7

formulated the idea that there exists one primeval matter and two pairs of qualities: hot/cold and wetness/dryness. As these qualities are impressed on the primeval matter, four elements were thought to be produced: fire (hot + dry), air (hot + wet), earth (cold + dry), and water (cold + wet). All material things are then the different combinations of these four elements. it is not difficult today to extract the roots of the theory, namely heat is equated with 'fire' and the other three 'elements' are the traditional three macroscopic phases: gas, solid, and liquid, respectively. A self-consistent, continuum theory of matter was thus created based exclusively on macroscopic experiences.

In addition, Greek philosophers also made an effort to develop atomic theories to speculate about the microscopic structure of matter. Anaxagoras and Empedocles suggested that matter is composed of infinitely small seeds. Even closer to present-day knowledge is the proposal of Leucippus and Democritus of the 5th century BC. It asserts that matter consists of indivisible atoms moving rapidly and at random in a void. Criticism by Plato and Aristotle caused the atomic theory, however, to be neglected for over 2000 years, until experimental proof became possible at the beginning of the 19th century.

This proof of an atomic theory of matter is credited to Dalton [2]. He extracted the constant combining ratios of elements to compounds from measurements of constant changes in ratios of weight of reactants and products during chemical reactions. Modern science has since established the detailed atomic and molecular of matter. The microscopic length scale, the ångström (0.1 nm), is based on the diameter of atoms and is $\approx 10^{-4}$ times the smallest macroscopically[4] recognizable length, the micrometer. With this large jump from macroscopic observation to microscopic structure completed, a logical subdivision of all matter into three classes is possible [3]. Fig. 1 illustrates this scheme, including some of the basic properties of the molecules and an operational definition of the solid state.

Quantitative experiments with heat, Q, began after the invention of reliable, closed-capillary, liquid-in-glass *thermometers* in Florence in the 17th century. Somewhat later, Richmann established in 1747 the calorimetric mixing formula that expresses how bodies at different temperature, T, come to equilibrium at an intermediate temperature. By following discrepancies between experimental values and results expected from Richmann's formula, Black and Wilcke, independently, discovered phenomena that led to the concepts of *latent heat* and *heat capacity*. Latent heat is absorbed without change in temperature, and heat capacity is the heat needed to increase temperature by one unit (kelvin), as defined in Eq. (1), in the following.

Toward the end of the 18th century, one began to consider the analytic consequences of the (erroneous) assumption that there may be a material basis of heat, which was called the *caloric*. A quote from Lavoisier [4] illustrates the difficulties experienced at that time: "This substance (meaning the caloric), whatever it is, being the cause of heat, or, in other words, the sensation which we call *warmth* being caused by the accumulation of this substance, we cannot, in strict language distinguish it by the term *heat*; because the same name would then very improperly express both cause and effect...." Even today we have not improved our language to clearly distinguish cause and effect.[5] The caloric theory gave, however, a satisfactory quantitative account of calorimetry. Even heat conduction could be fully described (Fourier, 1822) without specifying the true nature of heat.

Another mathematical theory of the caloric was given by Carnot (1824), based on the efficiency of a *reversible* heat engine, which seemed to rest on the assumption of a conserved material of heat. Count Rumford, however, had inferred already in 1798 from the high temperature reached on boring cannon barrels that heat is created by friction and not conserved. His qualitative arguments were, however, not convincing enough to upset the acceptance of the caloric theory.

[4]Macroscopic systems are recognizable directly on a human scale. Particles of micrometer size can be 'seen', for example, by the light they diffract (dust particles in strong sunlight) or under an optical microscope. Microscopic systems, in contrast, are of atomic size and need special magnification, such as are possible with an electron microscope or by X-ray diffraction.

[5]One still says, for example, the heat in this room is unbearable when one means the temperature is unbearable. Temperature, T, is the intensive parameter of heat, defined as the partial differential of energy, U, with rspect to entropy, S, without exchange of work ($T = \partial U/\partial S$).

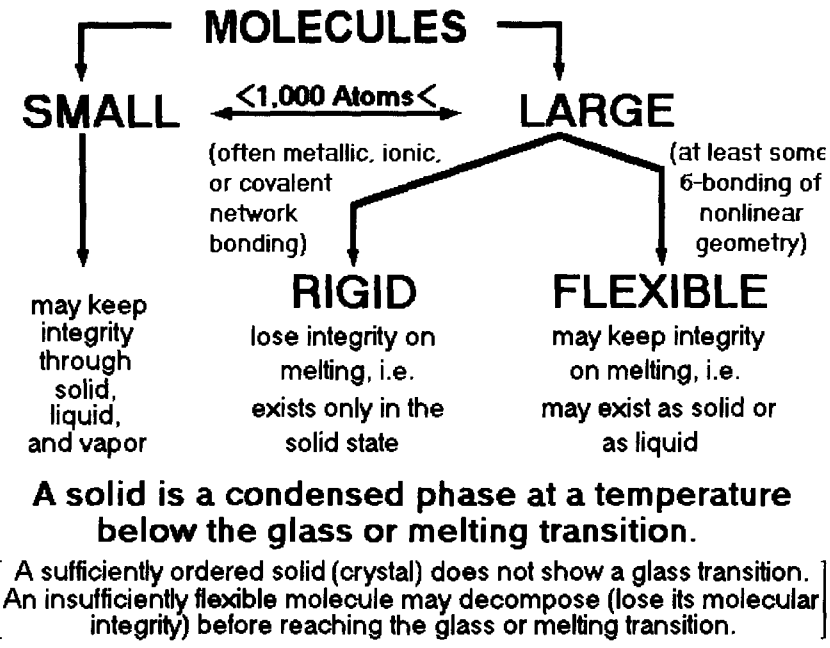

Fig. 1. Schematic of the three classes of molecules as linked to their possible phase structures [3]. Large molecules, called macromolecules, may consist of sufficient atoms to be single-molecule phases. Flexible macromolecules are often called polymers and may easily cross phase boundaries.

This was achieved only by the quantitative experiments of Joule in the 1840s who proved that the energy of an electric current can produce either heat *or* mechanical work, each with a constant conversion factor. From these experiments, he inferred properly that heat was a state of motion, not a material. In the early 1850s, this conflict was finally resolved by Kelvin and Clausius, who independently recognized that two distinct principles had been misconstrued. Joule had correctly asserted that heat could be created and destroyed in proportion to the exchanged amount of mechanical, electrical, or chemical energy, w (First Law of Thermodynamics – the total energy of a system is conserved: $dU = \delta Q + \delta w$); but Carnot's result also holds, it rests not on the conservation of heat but of entropy (under reversible conditions, the change in entropy is zero: $\Delta S \equiv Q/T = 0$, Second Law of Thermodynamics).

Today it is easy to represent the atomic motion by molecular dynamics simulation using supercomputers. Fig. 2 shows an example of a representation of the skeletal motion of a polyethylene crystal at low temperature [5]. This vibrational motion was linked by Einstein [6] and Debye [7] early this century to the basic quantity of calorimetry, the heat capacity ($C_v = \partial U/\partial T$ at constant volume, and composition). The total energy ($U = \int C_v dT$) is represented by the Hamiltonian of the crystal, and the temperature can be extracted from the kinetic energy ($3kT/2 = \sum mv^2/2$, where the sum is taken over the kinetic energy of all atoms of the system; m is the atomic mass, v the atomic velocity and k the Boltzmann constant). The time scale of atomic motion is the picosecond (10^{-12} s), far removed from the fastest event macroscopically perceivable, the millisecond (factor 10^9).

Perhaps this difference of five orders of magnitude in distance, from human level of experience, between molecular motion and structure is the reason for the relatively slow development of calorimetry based on thermodynamics and its link to molecular structure and motion. For a full description of a material, this structure and motion must be known on a macroscopic level through mass and calorimetric data, and on a microscopic level through molecular structure and mobility data. It will be shown below, that phase

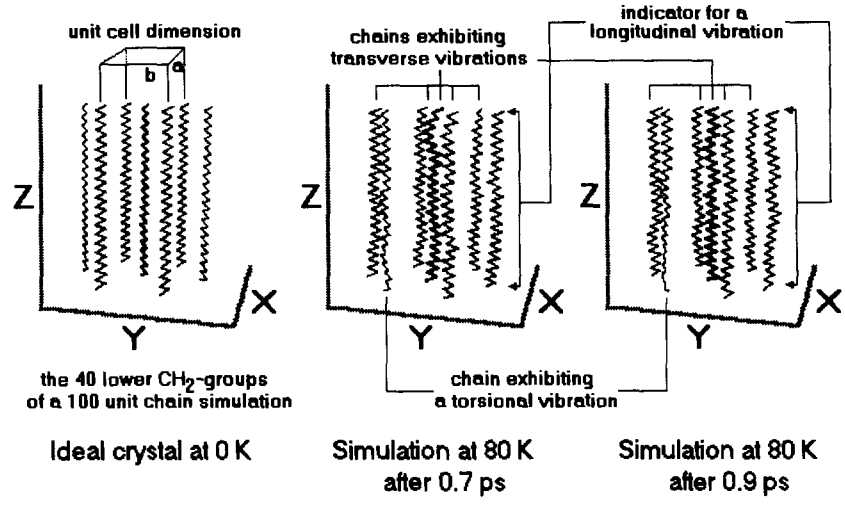

Fig. 2. Snapshots of molecular motion resulting from molecular dynamics simulation of polyethylene crystals [5].

structure and molecular structure – once thought of as corresponding to microscopic and macroscopic structure – may be overlapping when dealing with macromolecules and nanophases.

3. Development of calorimetry

The definition of heat capacity at constant pressure C_p, is given by:

$$C_p \equiv \frac{dQ}{dT} = \left(\frac{\partial H}{\partial T}\right)_{p,n} \quad (1)$$

with Q representing the heat exchanged, H the enthalpy, and the subscripts 'p' and 'n' signifying the conditions of constant pressure and composition. The dimension of C_p is $J\,K^{-1}\,mol^{-1}$, or for the specific heat capacity $J\,K^{-1}\,g^{-1}$. The basic measurement involves, thus, the determination of the amount of heat needed to raise the temperature by a given amount $(\Delta Q/\Delta T)$.

Good calorimetry was already carried out in the 18th century, as shown in Fig. 3 and described by Lavoisier [4]. Heat was measured by finding the heat flow to the measuring ice in volume 'HGbbd' from a sample of known, higher temperature T_1, in basket 'LM' which is inserted into the calorimeter cavity 'ff'. The whole calorimeter was kept adiabatic by a second, insulating layer of ice in 'FFaaaa'. After equilibration,

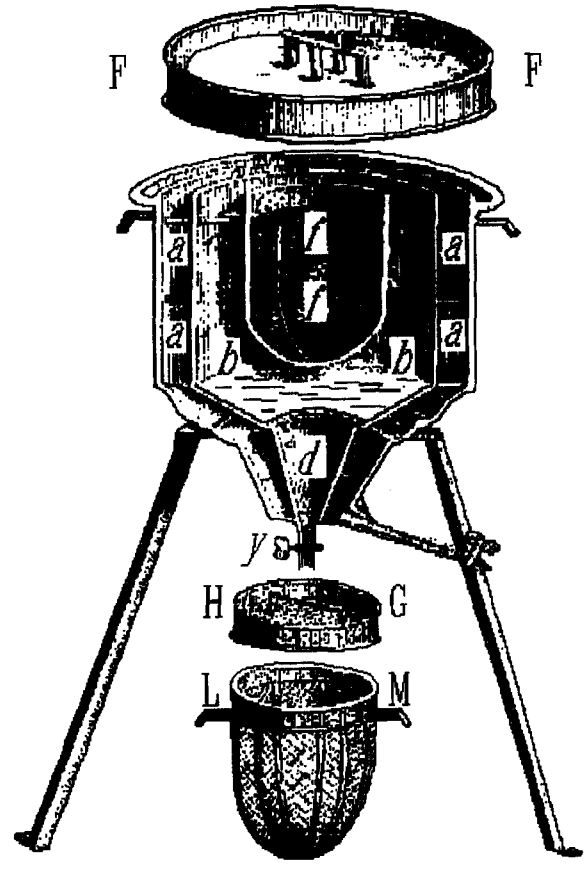

Fig. 3. Ice calorimeter of de la Place built in 1781. Total height of the calorimeter is ≈1 m [4].

which for larger samples might take as much as 12 h, the water was drawn through the stopcock and weighed. The average specific heat capacity of the sample, c_p, for a given mass m_{sample} was then given by:

$$c_p = \frac{m_{water}L}{m_{sample}(T_1 - T_0)} \quad (2)$$

where L is the latent heat of fusion of the unit mass of ice, and T_0 the melting temperature of ice. Many materials and even biological specimens, like living mice, were studied in this fashion.

Classically, the measurement of heat capacity is done with an adiabatic calorimeter [8]. Even today, adiabatic calorimetry is the most precise method of measurement in the (10–300) K temperature range (possible precision ±0.1%), and practically the only method used in the (10–150) K range [9]. In an adiabatic calorimeter, an attempt is made to follow the stepwise temperature change ΔT of an internally heated calorimeter in well-controlled, adiabatic surroundings. Corrections must be made for ΔQ due to the positive or negative heat flux caused by deviations from the adiabatic condition, and for ΔT due to overall temperature drifts of the calorimeter. The specific heat capacity c_p becomes thus:

$$c_p(\text{sample}) = \frac{\Delta Q_{corrected} - C'\Delta T_{corrected}}{\Delta T_{corrected} \times m_{sample}} \quad (3)$$

where C' is the heat capacity of the empty calorimeter, its 'water value', and m the mass of the sample [9]. An evaluation of the corrections is the most time-consuming part of the measurement and at the heart of good calorimetry (i.e. for measurements with better than ±1% precision).

In the 1950s and 1960s, major adiabatic calorimeters for measurements on polymers were in operation at the National Bureau of Standards [10] (now NIST), at Northwestern University [11], the GE Research Laboratory [12] and the University of Leeds, England [13]. A check of the literature [14] revealed, through 1955, only 30 papers on heat capacity of linear macromolecules, describing mainly natural and synthetic rubbers, polystyrene, poly(vinyl chloride), polyethylene, selenium, nylon 6, polytetrafluoroethylene,and polyfluorotrichloroethylene. The first papers on heat capacity of characterized polymers date back to 1928–1938 [15–18].

An extension of the theory of heat capacity of solids [6,7] to polymers was suggested by Tarasov [19]. A detailed analysis of the vibration characteristics of a polymer was made by Stockmayer and Hecht [20]. This means that, in the 1950s, a solid foundation existed for calorimetry of polymers. The limitations were that adiabatic calorimetry was a cumbersome and complicated technique, that most attempts to understanding the thermal properties of macromolecules used an equilibrium approach to describe nonequilibrium effect, and that the morphology of the polymers was not well-understood [21]. The next 25 years showed considerable progress on both topics and laid the foundation for the discussions to be given in the following [9,21,22].

4. Phases and transitions

A *phase* is a homogeneous volume of matter, separated by well-defined surfaces. Atoms and molecules are the building blocks of a phase and set the lower limits in size for the requested homogeneity. Over the years, three important size-ranges of phases have emerged. The first are *macroscopic phases*. They cover the sizes of over one micrometer in all directions and are well-described by thermodynamics. One of the important statements about macroscopic phases in equilibrium is the *phase rule*. The number of phases plus the number of independently variable functions of state (degrees of freedom, such as pressure, temperature, and concentrations) is equal to the number of components out of which the system can be generated, plus two ($P + F = C + 2$) [9]. Some additional statements about phases and molecules are already given in Fig. 1. Small molecules can assume different phases without loss of molecular integrity. Early problems to recognize the identical molecules in different phases are mirrored in our language. Ice, water, and steam are different names for the same H_2O molecules in different phases. By the time other substances were commonly available in different phases, this problem was resolved.

New difficulties arose when substances were identified that consist of phases in the second range of sizes, the colloids. Although inorganic and organic colloids were used since antiquity, Graham is regarded through his work in the 1860s as the

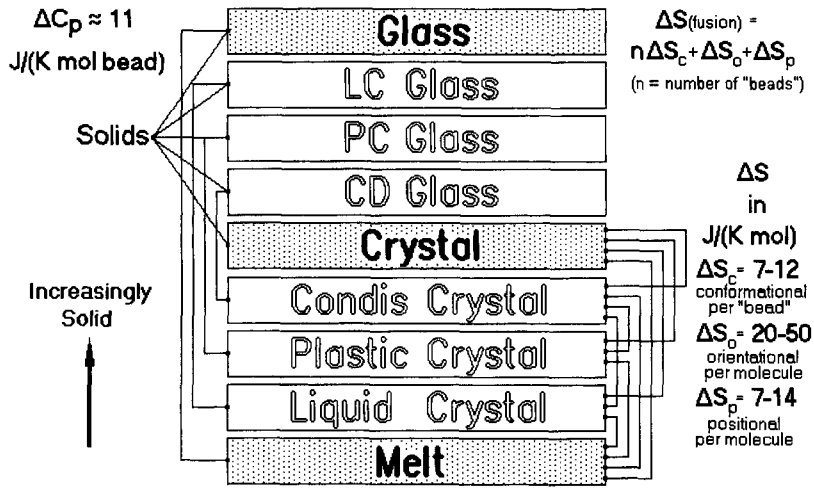

Fig. 4. Schematic of the classical phases (shaded boxes) and the mesophases. Transitions are indicated by the connections between the boxes. Orientational and positional entropy contributions refer to the whole molecule and are negligible for macromolecule. Conformational contributions depend on the number of rotatable parts of the molecule n (beads).

founder of what is called *colloid science*. Colloidal particles are *microphases*, i.e. they are smaller than about one micrometer. For their thermodynamic description surface properties must be considered as additional functions of state. Since early research established that organic colloidal phases may consist of small molecules, held together by weak, secondary forces, it was thought for a long time that flexible macromolecules which reach and exceed micrometer lengths were also aggregates of small molecules (rings to account for the stoichiometry of macromolecules). In fact, the true nature of polymers was generally accepted only after the work of Staudinger in the 1920s [1]. At this point, one recognizes that the size of phases may be small and the size of molecules large. From Fig. 1 it is easy, in hindsight, to see that the long-known colloidal gold, that typically consists of particles of 5–1000 atoms, certainly represents macromolecules since all gold atoms in one particle are linked by strong, metallic bonds, i.e. one phase area = one molecule. Similar statements can be made about other inorganic colloids, such as clays and metal hydroxides. Linear macromolecule or polymers cause additional complications since they may, because of their structure, easily cross phase boundaries and participate in more than one phase area. This was recognized initially through the study of semicrystalline polymers and is responsible for many of the special properties of flexible linear macromolecules [22,23].

The third size range of phases deals with the smallest colloidal particles, those that reach nanometer dimensions. These *nanophases* are so small that opposing surface interact. A thermodynamic description now becomes difficult since one does not find large-scale homogeneity on a nanometer scale on account of the molecular structure parameters varying close to surfaces, and the atomic structure itself limits homogeneity. Nanophase structures of polymers are particularly interesting since a single macromolecule can participate in several or many different phase areas. Special attention must be paid to the stability of microphases and nanophases. Only if the available material is limited, or the molecular structure forces phase areas of limited size, can equilibrium be reached. The properties are then fixed by surface and, perhaps, additional internal structure parameters[23]

The *types of condensed phases* of matter are categorized for thermal analysis in Fig. 4 [24]. The three classical phases are represented by the dotted boxes. Crystals are ordered solids that practically show only vibrations as thermal motion. Because of the order, their entropy vanishes when cooled to the absolute zero of temperature (third law of thermodynamics). The glasses are also solids with almost exclusively

vibrational motion, but they possess a disordered structure that is close to that of the liquid at the glass-transition temperature. They have a positive residual entropy at 0 K which, for linear macromolecules, is a measure of the conformational disorder and metastability. A series of 45 of such residual entropies has been measured and averages 6.1 J/(K mol of mobile segments of the molecule) [25,26]. The mobile segments are assumed to be the basic *beads* that characterize the various phases. For example, each bead contributes $\approx$11 J K^{-1} mol^{-1} to the heat-capacity increase when going from the glass to the liquid at the glass-transition temperature, T_g, as indicated on the left side of Fig. 4 [26,27]. Since the structure of the glass does not change on devitrification, the entropy and enthalpy do not change at the glass transition.

The increase in heat capacity on devitrification is caused by the beginning of large-amplitude motion that is characteristic of the liquid. Three major types of large-amplitude motion are possible: translation of the molecule as a whole (also called positional motion), orientational motion (also based on motion of the whole molecule), and conformational motion (the internal rotation of the various segments of flexible molecules). All three degrees of freedom of large-amplitude motion freeze on vitrification to their corresponding skeletal vibration as illustrated in Fig. 2.

The transitions marked on the right-hand side of Fig. 4 involve a change in order (i.e. entropy) and enthalpy. In view of these changes on transition, they are called first-order transitions [28]. When a crystal melts, a similar gain of large-amplitude motion is observed as for the glass on devitrification, but since the heat capacity of solid macromolecules always increases more with temperature than the heat capacity of liquids, the increase in heat capacity on fusion is less than at the glass-transition temperature.

A large number of entropies of fusion have been collected and correlated with the molecular and crystal structure. These data revealed that the different large-amplitude motions, coupled with the corresponding disorder, contribute well-defined entropies of fusion, as written on the right-hand side of Fig. 4 [3,9]. The translational or positional entropy contribution to the entropy of fusion is 7–14 J K^{-1} mol^{-1}, as already expressed some 100 years ago by Richards' rule [29]. The positional entropy is observed as total entropy of fusion for crystals with spherical motifs, such as metals and the noble gases. Crystals of rigid, nonspherical motifs have an additional orientational contribution of 20–50 J/(K mol) for the entropy of fusion. This empirical rule was already suggested by Walden [30].

The equilibrium entropies of flexible macromolecules have, because of their high molar mass (> 10 000) [1], only a negligible positional and orientational molar entropy of fusion. Practically all of the entropy of fusion is conformational. A large selection of extrapolated and measured entropies of fusion [3,9] revealed typical conformational entropies of fusion of 7–12 J K^{-1} (mol of beads)$^{-1}$. Within the rather large, empirically established limits, first-order transition entropies can be linked to changes in molecular structure. All other contributions to the transitions, such as coming from changes in vibrational frequencies, volume, short-range order, conductivity, etc. are smaller and sufficiently coupled to the large-amplitude motions so that no additional contributions are needed to characterize the overall entropy of fusion.

For quite some time it is known, however, that intermediate phases, called *mesophases*, exist. In these mesophases, one, or more, of the types of order of the crystal is missing and the corresponding large-amplitude motion characterizes the physical properties. The mesophase known for the longest time is the *liquid crystal*, discovered ca. 1900 [31]. In classical, *thermotropic liquid crystals*, some orientational order is introduced into the liquid phase due to a rod, disc, or boardlike molecular structure, the mesogen, as a part of the molecule that permits easy parallel arrangement (loss of entropy). The orientational ordering is coupled, because of the shape of the mesogen, with a relatively small loss of enthalpy, so that the phase transition to the liquid occurs at a sufficient high temperature to produce a stable mesophase. The order of a liquid crystal is easily observed by its birefringence and the fact that the overall appearance of the phase remains liquid-like [32]. The entropy gain on isotropization of such liquid crystal may be as little as 2.1 J/(k mol) (nematic liquid crystals, average of 278 low molar mass liquid crystals, compared to that in Fig. 4).

Amphiphilic liquid crystals gain their liquid crystalline superstructure by the existence of a phase bound-

ary between asimilar segments of a molecule [32]. If the phase domains are of micrometer dimensions, the order introduced by the interphase dissipates within the phases. Both phases may then be amorphous, exhibiting independent glass transitions, or one or both may crystallize with only minor restrictions caused by the interphase. As the phase areas become of nanometer dimensions, the order introduced by the interface does not dissipate anymore and orientational and conformational order may exist without the presence of a mesogen. Typical examples of small molecules with such structures are neat soaps, lipids, and partially perfluorinated paraffins. In macromolecules, amphiphilic liquid crystals of nanometer phase dimensions may form with conformational order in flexible segments, similar to thermotropic liquid crystals, but without mesogen [32].

A mesophase with a larger degree of order is the *plastic crystal* [33]. Plastic crystals are frequent for molecules of close-to-spherical shape which start orientational motion and disordering within the crystal without loss of positional order. They were discovered in the 1930s. Besides their plasticity, they show only positional entropy on isotropization [7–14 $J\,K^{-1}\,mol^{-1}$] and a close-packed cubic crystal structure [33]. Typical examples of plastic crystals are carbon monoxide (CO), neopentane [$C(CH_3)_4$], and fullerene (C_{60}). Their molecular motion consists of rotations in addition to the vibrations found in solids.

For linear macromolecules, the orientational disorder of the molecule as a whole is replaced by segment (bead) mobility which leads to conformational disorder. The mesophase is called conformationally disordered [34] and the crystal are called *condis crystals* [24,35]. Their entropy of isotropization is linked to the remaining conformational order, and varies from crystal to crystal. For polyethylene, which has a condis phase at elevated pressures, the entropy of isotropization is $\approx 2\ J\,K^{-1}$ (mol of CH_2)$^{-1}$, while for polytetrafluoroethylene the entropy of isotropization is 6.8 $J\,K^{-1}$ (mol of CF_2)$^{-1}$. The overall entropy of fusion of both polymers is about the same, (10 $J\,K^{-1}\,mol^{-1}$). The conformational mobility accounts for easy chain extension after chain-folded crystallization and also for the special frictional properties (low shear viscosity in the chain direction of the crystal) [35].

The possible transitions of the mesophases to higher and lower degrees of order are indicated on the right-hand side of Fig. 4 and the corresponding entropies of transition can be estimated from the listed empirical rules. In case the mesophase is hindered on further ordering on cooling, either due to quenching or intrinsic hindrance, a corresponding glass is formed, as shown on the left-hand side of Fig. 4. In the mesophase glasses, the order is the same as in the mesophase, but the large-amplitude motion has changed into skeletal vibration. All three types of mesophase glasses have been observed [24,35].

5. Temperature modulated calorimetry

Modern control and measurement technology permitted, some 30–40 years ago, miniaturization of the calorimeter to measure down to milligram quantities in a continuous, scanning mode and to change from an adiabatic to an isoperibol environment [36]. Twin calorimetry was needed to simplify the heat-flux corrections Eq. (3) by measuring in a differential mode between a sample and a reference calorimeter. In a symmetric setup, the difference in extraneous heat flux could be minimized and the remaining imbalance corrected for. This type of instrument is the well-known *differential scanning calorimeter*, DSC, which responds quickly and can not only measure the calorimetric responses, but may also identify the kinetics of irreversible processes [37]. Under the usual condition where sample and reference calorimeters (often aluminum pans) are identical, and the reference pan is empty, one finds the heat capacity as [9]:

$$mc_p \approx K\frac{\langle \Delta T\rangle}{\langle q\rangle} \tag{4}$$

where K is the Newton's law constant, $\langle \Delta T\rangle$ the temperature difference between reference and sample $(T_r - T_s)$ without the later discussed modulation effect, and $\langle q\rangle$ the constant, underlying heating rate. Eq. (4) is exact if sample and reference calorimeters are heated at the same rate (steady-state and constant c_p, resulting in a horizontal DSC-curve). For the case of changing heating rate of the sample due to a slowly changing heat capacity, easy corrections are available [9], but are often neglected for measurement with precision of $\pm 3\%$ or less.

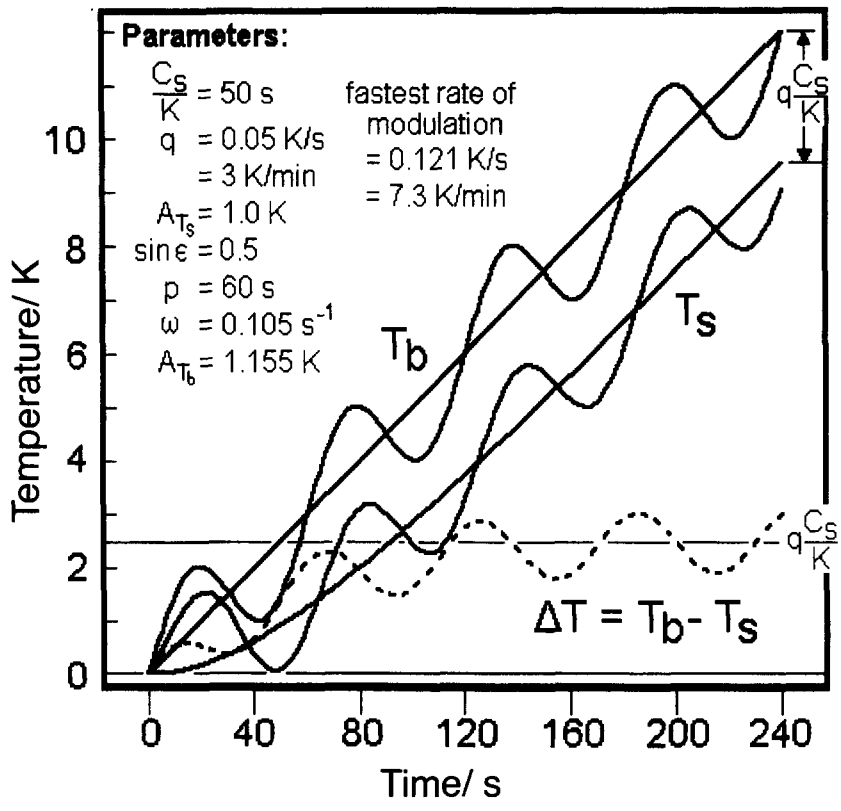

Fig. 5. Calculated change of the block and sample temperatures at the beginning of a TMDSC experiment showing the approach to steady state. the averages (heavy, not modulated lines) apply to standard DSC and correspond to averages over one modulation cycle.

In the very recently developed *temperature-modulated DSC* (TMDSC) a sinusoidal or other periodic change in temperature is superimposed on the underlying heating rate $\langle q \rangle$ [38]. The sample temperature, under these conditions, is given by:

$$T_s(t) = T_0 + \langle q \rangle t - \langle q \rangle \frac{C_s}{K} + A \sin(\omega t - \varepsilon) \tag{5}$$

where T_0 is the temperature at the start of the experiment, C_s the heat capacity of the sample calorimeter (sample + pan), A the maximum amplitude of the sample-temperature modulation, and ω the modulation frequency $2\pi/p$(p = modulation period in seconds). Analogous equations hold for the reference temperature, T_r (maximum amplitude A_r and phase shift ϕ) and the temperature difference, $\Delta T = T_r - T_s$ (maximum amplitude A_Δ and phase shift δ) [39]. The standard DSC can be thought of as TMDSC without modulation ($A = 0$).

The conditions for the approach of the calorimeter to steady state have been explored [40]. A typical approach to steady state of the sample temperature T_s at the beginning of a run is illustrated in Fig. 5 for the standard DSC (heavy lines without modulation) and TMDSC (modulated traces). Analogous curves can be derived for T_r and ΔT. Small samples can be studied by TMDSC over at least one order of magnitude of change in time scale [41].

Experiments with modulation *and* an underlying linear heating rate, as shown in Fig. 5, have two time scales, one due to the underlying heating rate and the other due to modulation. Each can be used for measurement of heat capacity. As long as the heat capacity is independent of time, as is usually the case, both evaluations give the same result.

The determination of the heat capacity from modulation alone is carried out by a *pseudo-isothermal analysis*. The effect of modulation is separated for this analysis from the underlying change in temperature due to the heating rate $\langle q \rangle$ seen in Fig. 5. The change in ΔT, for example, is given by $\Delta T(t) - \langle \Delta T \rangle$, where the average $\langle\ \rangle$ is always carried over $\pm(1/2)p$, so that any sinusoidal effect averages to zero and the difference gives the required effect due to modulation alone. Evalutation of the calibration constant and the maximum amplitude of the temperature difference, A_Δ, which is proportional to the maximum heat-flow amplitude A_{HF}, gives the heat capacity [39]:

$$mc_p \equiv \frac{A_\Delta}{A}\sqrt{\left(\frac{K}{\omega}\right)^2 + C'^2} = \frac{A_{HF}}{A} \times K' \qquad (6)$$

where A and ω are parameters set at the beginning of the experiment and described in Eq. (5), and C' the heat capacity of the empty reference pan of identical mass to the empty sample pan. The calibration constant K is independent of modulation frequency and reference heat capacity. The commonly measured calibration constant K' changes for runs with different ω and C' (K' is sometimes also written as K''/ω). Eq. (6) represents the *reversing heat capacity*. It can then be compared to the heat capacity measured from the underlying heating rate $\langle q \rangle$ alone, making use of the total heat flux $\langle HF \rangle$, or temperature difference $\langle \Delta T \rangle$, as calculated from Eq. (4) and seen in Fig. 5. In case there is a difference between the result of Eqs. (4) and (6), this is called the *nonreversing heat capacity*, and is connected to a process that cannot be modulated within the sample, such as irreversible crystallization and reorganization, or heat losses.

A third experimental mode of measuring C_p by TMDSC is possible by keeping the average temperature, $\langle T \rangle$, constant, at T_0. This mode is called *quasi-isothermal analysis* [37]. To cover a range of temperature, separate experiments must be done at every T_0, similar to the adiabatic analysis of Eq. (3). This analysis mode is more time-consuming, but has the advantage that steady state can be awaited and any inaccuracies in separating the effects from the two time scales is avoided. The heat capacity is given in this case also by Eq. (6). Typically, runs of 20-minute duration are made at each temperature and the last 10 min are used for data collection and analysis. Using one data point at intervals of 10 K, 200 K can be covered in seven hours.

With this wide range of calorimetric techniques it is now possible to establish the equilibrium heat capacities [26] as well as the apparent, frequency-dependent heat capacities that are found, for example, in the glass-transition region [42]. Latent heats are usually recognized by their much larger endothermic or exothermic effects concentrated in *transition regions*. The equilibrium melting of polyethylene absorbs, for example, $4100\,J\,mol^{-1}$ over a few kelvins, while the heat capacity of liquid polyethylene is $38.8\,J\,K^{-1}\,mol^{-1}$. Such enormous differences in heat effect are easily separated by finding a baseline that represents the heat capacity and using the endotherm as measure of the heat of transition [9]. Polymers, however, can often show broad transition regions as well as transitions of small heat effects (see Fig. 4). In these cases independent information on heat capacity must be available. The *Advanced THermal Analysis System*, ATHAS, was developed for this purpose and is described next [43].

6. Heat capacity

The interpretation of the *heat capacities of solids* developed in four major steps. First, it was observed empirically by Dulong and Petit, in 1819, that the heat capacities of solids at room temperature and at higher temperatures are often $C_v = NR$, where N is the number of degrees of freedom of vibrations (three times the number of atoms) and R the gas constant, given in SI units as $8.314\,J\,K^{-1}\,mol^{-1}$. In the early 19th century, this rule helped often to establish molar masses, particularly for metals.

Some 100 years later, Einstein [6] showed the connection between heat capacities of solids and their vibrations. The observed decrease in heat capacity from the Dulong–Petit rule at lower temperatures is due to the insufficient excitation of vibrations that need to be described by quantum mechanics. The Einstein function $E(\Theta_E/T)$ is given by:

$$C_v/NR \equiv E(\Theta_E/T) = \int_0^{(\Theta_E/T)} \frac{(\Theta_E/T)^2 \exp(\Theta_E/T)}{[\exp(\Theta_E/T) - 1]^2} \qquad (7)$$

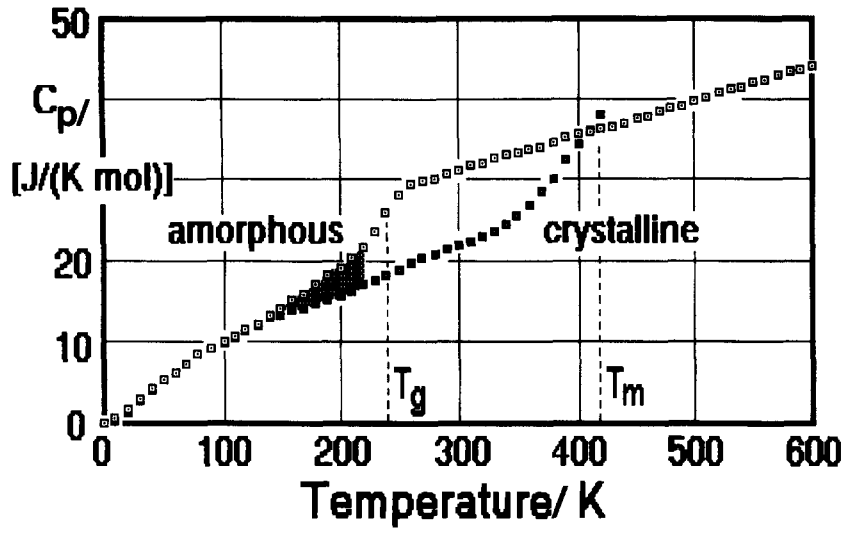

Fig. 6. Extrapolated experimental heat capacities of polyethylene to the amorphous and crystalline phases. For data see [26]. The glass transition is at 237 K, the melting transition at 414.6 K.

where N is the number of vibrational degrees of freedom, and Θ_E the Einstein temperature, characteristic for the average frequency that describes the vibrations in the solid. The conversion factors from frequency in Hz and cm^{-1} to Θ-temperature in kelvin are: 4.80×10^{-11} K Hz^{-1}, and 1.44 K cm, respectively.

Debye, shortly thereafter [7], developed a theory based on a continuous vibrational spectrum as one observes for macroscopic bodies, but cut at a low frequency where the number of vibrations reaches N:

$$C_v/NR \equiv D_3(\Theta_3/T) = 3(T/\Theta_3)^3 \times \int_0^{(\Theta_3/T)} \frac{(\Theta/T)^4 \exp(\Theta/T)}{[\exp(\Theta/T) - 1]^2} d(\Theta/T) \quad (8)$$

where $D_3(\Theta_3/T)$ is the Debye function for three-dimensionally continuous solids. The heat capacity of many metals and salts can be described by this theory with a single parameter, the Θ-temperature. The final step in an understanding of the heat capacities of solids involves the use of the actual vibration spectrum of the solid [44].

Several problems arise for polymers because of linear structure of the molecule and the different groups attached to the backbone chain. Fig. 6 shows the experimental heat capacities for polyethylene extrapolated to the completely amorphous and crystalline states. The T^3-dependence of the heat capacity which is characteristic of a continuous vibrational spectrum, as assumed by Debye, holds for the crystalline polyethylene only between 0 and 10 K [45]. Next, there is a change to a linear temperature dependence of the heat capacity. For the crystalline polyethylene, this linear increase in heat capacity continues to ≈300 K. Such temperature dependency fits a one-dimensional Debye function which is based on a constant number of vibrators over a range of frequencies going from 0 to Θ_1 [46], with Θ_1, again, representing a characteristic frequency (temperature):

$$C_v/NR \equiv D_1(\Theta_1/T) = (T/\Theta_1) \times \int_0^{(\Theta_1/T)} \frac{(\Theta/T)^2 \exp(\Theta/T)}{[\exp(\Theta/T) - 1]^2} d(\Theta/T) \quad (9)$$

At ≈250 K, one notices in Fig. 6 a slowing of the increase of the crystalline heat capacity with temperature and a renewed increase occurs ≈300 K, to reach close to the melting temperature values equal to, and higher than the heat capacity of liquid polyethylene.

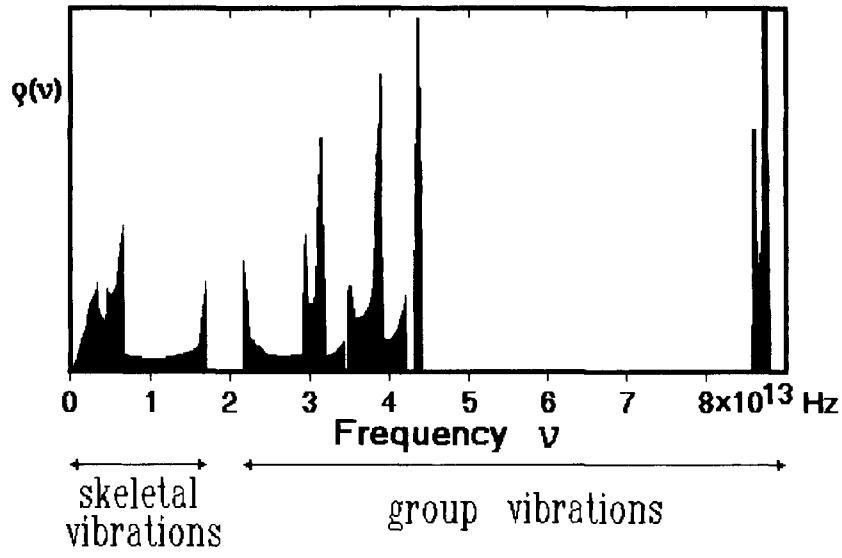

Fig. 7. Vibrational spectrum of crystalline polyethylene, derived from normal mode calculations as described in [49]. The number of vibrators at each frequency ν is given by $\rho(\nu)$.

The heat capacity of the glassy polyethylene at low temperatures is higher than the heat capacity of the crystal and not strictly describable by a constant Θ_3. At these temperatures, the absolute value of the heat capacity is, however, small and an approximation with a lower Θ_3 than that for the crystal is possible (80 K vs. 158 K, respectively, see Fig. 6). After a long temperature range of heat capacities close to those of crystal and glass, the glass transition occurs at 237 K. A small increase in the amorphous heat capacity beyond the values of the crystals starts already at $\approx$110 K and the heat capacity contribution that is shaded in Fig. 6 has been linked to the γ-transition that is caused by local conformational motion [47]. In the liquid state, the heat capacity is approximately linear over a very wide temperature region. Much less is known about the motion in the liquid than in the solid [48].

The quite complicated temperature dependence of the solid heat capacity is to be linked next to a more detailed, approximate microscopic model of thermal motion. The basic equations linking vibrational frequencies to heat capacity are the Einstein function, Eq. (7), and the Debye functions, Eqs. (8) and (9). As an initial try, one can invert the vibrational spectrum of crystalline polyethylene, known in some detail from normal mode calculations, using force constants derived from infrared and Raman spectroscopy [49] and represented in Fig. 7. Using a different Einstein function for each normal mode vibration, one can compute a heat capacity, but only above $\approx$50 K does the calculation and measurement agree. Below 50 K, the experimental data show increasing deviations, an indication that the computation of the low-frequency skeletal vibrations cannot be carried out with sufficient precision [50]. To overcome the error in C_v when computed from the low-vibration frequencies, the method of generating approximate spectra was developed, as will be described next.

For polyethylene and most other polymers, one can distinguish between skeletal and group vibrations. The first reach from 0 to $\approx 2 \times 10^{13}$ Hz as marked in Fig. 7. Polyethylene shows two degrees of freedom (N) in this frequency range. The motion involved in these vibrations can be visualized as torsional and accordion-like motions of the CH_2-backbone. Torsion involves mainly bond rotation, whereas the accordion-like motion involves bending of the C–C–C-bonds. Their frequencies are such that they contribute mainly to the increase in heat capacity from 0 to 200 K.

The group vibrations occur at a somewhat higher frequency. This gap in the frequency distribution in

Fig. 6 is responsible for the leveling of the heat capacity at ≈250 K (see Fig. 6). In the plateau region, C_p is of the proper order of magnitude for the assumed two degrees of freedom (i.e. ≈16–17 J K^{-1} mol^{-1} or $2R$).

The *group vibrations* originate from the relatively isolated groupings of atoms along the backbone chain. In the first set of group vibrations, between 2 and 5×10^{13} Hz, there are five degrees of freedom, involving mainly C–H-bending and C–C-stretching motions. The stretching vibration of the C–C-bond falls into the same frequency range as the C–H-bending. Due to the close-to-90° bond angle (110°) the C–C-stretching is not coupled sufficiently along the chain and is thus included in the group vibrations. These latter five vibrations are responsible for the renewed increase of the heat capacity in Fig. 6, starting at ≈300 K. Below 200 K, their contributions to the heat capacity are small.

Finally, the CH_2-groups have two more group vibrations of very high frequencies, $> 8 \times 10^{13}$ Hz. These are the C–H-stretching vibrations and are so high, that at 400 K their contribution to the heat capacity is still small. The total of nine vibrations possible for the three atoms of the CH_2-unit would, when fully excited, lead to a heat capacity of 75 J K^{-1} mol^{-1}. At the melting temperature, only half of these vibrations are excited, so that C_v is ≈38 J K^{-1} mol^{-1}.

A full analysis and computation of heat capacities involves the following steps: The experimental heat capacities are, if necessary, first extrapolated to the fully amorphous or crystalline state, with results as shown in Fig. 6. These heat capacities are, naturally, measured at constant pressure, i.e. are C_p, as defined by Eq. (1), while the calculations yield the heat capacity at constant volume, C_v. Their conservation is accomplished using standard thermodynamic relationships or, if compressibility and expansivity needed for the conversion are not available, the Nernst–Lindemann approximation applied to the case of polymers [51]:

$$C_p - C_v = 3RA_0C_pT/T_m^0 \tag{10}$$

with T_m^0 representing the equilibrium melting temperature, and $A_0 = 3.9 \times 10^{-3}$ J^{-1} K mol, an approximately universal constant. The total experimental C_v is then separated into the part due to the group vibrations and another due to the skeletal vibrations:

$$C_v(\text{total}) = C_v(\text{skeletal}) + C_v(\text{group vibrations}) \tag{11}$$

Table 1
Approximate frequency spectra for polyoxide group vibrations

Vibration type		Frequency in K	Number of vibrators
CH_2 symmetric stretch	Θ_E	4285	1.00
CH_2 asymmetric stretch	Θ_E	4168	1.00
CH_2 bending	Θ_E	2104	1.00
CH_2 wagging	Θ_E	2019	1.00
CH_2 twisting	Θ_E	1922	1.00
CH_2 rocking	Θ_E	1525	0.20
	Θ_E	1707	0.24
	Θ_L, Θ_U	1525, 1707	0.56
C–O-stretching	Θ_E	1385	0.22
	Θ_E	1632	0.11
	Θ_L,Θ_U	1685, 1632	0.67
	Θ_E	1305	1.00
C–C-stretching	Θ_L, Θ_U	1378, 1638	0.34
	Θ_L,Θ_U	1378, 1525	0.35
	Θ_E	1079	0.31

The heat capacity due to the group vibrations is calculated from an approximate spectrum obtained independently, as already discussed for polyethylene, and listed for poly(oxymethylene) [$(CH_2–O–)_x$] in Table 1 [52]. The group vibration of polyethylene can also be taken from Table 1, since their frequencies (as group vibrations) change only a little on introducing the ether oxygen. Similarly, the group vibrations for other aliphatic oxides can be determined with the help of Table 1. To increase the precision, some of the group vibrations that spread over a wider frequency range are approximated by box-distributions $B(\Theta_U/T, \Theta_L/T)$. The heat capacity contribution is computed with the help of two one-dimensional Debye functions of Eq. (9):

$$\begin{aligned} C_v/NR &\equiv B(\Theta_U/T, \Theta_L/T) \\ &= \frac{\Theta_U}{\Theta_U - \Theta_L}[D_1(\Theta_U/T) \\ &\quad - (\Theta_L/\Theta_U)D_1(\Theta_L/T)] \end{aligned} \tag{12}$$

The lower frequency limit is given by Θ_L, the upper one by Θ_U. Subtraction of all heat-capacity contributions of the group vibrations from the measured C_v

yield the experimental, skeletal heat-capacity contribution of Eq. (11).

The last step in the *ATHAS* analysis is to assess the skeletal heat capacity. The *skeletal vibrations* are coupled in such a way that their distributions stretch usually to zero frequency (i.e. to the acoustic vibrations). In the lowest frequency region one must, in addition, consider that the vibrations will couple intermolecularly. The wavelengths of the vibrations become larger than the molecular anisotropy of the chain structure. As a result, the detailed molecular arrangement is of little consequence at these lowest frequencies. A three-dimensional Debye function as written in Eq. (8) should apply. Only above this frequency range, the linearity of the molecules suggest a constant number of vibrations for each frequency. To approximate all skeletal vibrations of linear macromolecules, one should thus start out at low frequencies with a three-dimensional Debye function of Eq. (8) and then switch to a one-dimensional Debye function Eq. (9). Such an approach was derived by Tarasov [19]. The skeletal vibration frequencies are, thus, separated into two groups, the intermolecular group between zero and ν_3, (characterized by a three-dimensional Θ-temperature, Θ_3), and an intramolecular group between ν_3 and ν_1 (characterized by a one-dimensional Θ-temperature, Θ_1):

$$C_v/NR \equiv T(\Theta_1/T, \Theta_3/T) = D_1(\Theta_1/T) - (\Theta_3/\Theta_1)[D_1(\Theta_3/T) - D_3(\Theta_3/T)] \quad (13)$$

The fraction of vibrators in the intermolecular part is Θ_3/Θ_1, so that one has only two adjustable parameter. The approximate frequency distribution is thus fitted to the experimental skeletal C_v at low temperatures to get Θ_3 (0 to Θ_3 K) and at higher temperatures, to get Θ_1 (Θ_3 to Θ_1 K). More precise computer programs that accomplish the fitting over the whole temperature region are available [53]. Even neural network computations have been used for the evaluation of the Θ-temperatures [54]. Fitted values for the skeletal spectrum for some aliphatic polyoxides and polyethylene are listed in Table 2. The skeletal vibrations for other polyoxides and copolymers of CH_2- and ether-groups can be estimated from the data of Table 2 by interpolation [52]. The frequencies of the C–O–C-bending are available from normal-mode calculations, and are thus excluded from the Tarasov treatment. With Table 2 of the skeletal vibrations and Table 1 of group vibration frequencies, it is now possible, in turn, to calculate C_v, and with help of Eq. (10) also C_p.

Table 2
Approximate frequency spectra for polyoxide skeletal vibrations

Vibration type		Frequency in K	Number of vibrators
Polyethylene	Θ_1, Θ_3	519, 158	2.00
Poly(oxymethylene)	Θ_1, Θ_3	232, 117	2.00
Poly(oxyethylene)	Θ_1, Θ_3	353, 114	3.00
Poly(oxytrimethylene)	Θ_1, Θ_3	433, 101	4.00
Poly(oxytetramethylene)	Θ_1, Θ_3	436, 93	5.00
C–O–C-chain bending	Θ_E	870	1.00
	Θ_E	655	0.23
	Θ_L,Θ_U	360, 440	0.29
	Θ_L, Θ_U	360, 655	0.48

The precision of the heat capacities computed from the approximate frequency spectra is for most polymers better than ±5%. The computations can cover a temperature range beyond the experimentally available data and are fitted to the experiment only with two constants. They represent the heat capacity expected if all thermal motion in the polymer consists only of vibrations. Figure 8 shows such calculations for crystalline polyethylene. The contribution of the skeletal and group vibrations, as well as C_p and C_v are shown separately. References to detailed discussions of the approximate spectra fitted to experimental heat capacities for over 100 other polymers are given in the *ATHAS* data bank [55].

One of the important applications of the computed heat capacities over the full temperature range lies in comparison with the experimental data, as shown in Fig. 8. The first deviation from the vibration-only heat capacity is seen at ≈(250–300) K, as indicated by the shaded area. These deviations are linked to large-amplitude conformational motion and disorder which could be studied by molecular dynamics simulations and has given valuable information about the deformation mechanisms of crystalline polymers [5]. Similar large-amplitude motion effects can be seen for amorphous polyethylene in Fig. 6, starting already at ≈110 K, and were earlier linked to the γ-transition, observable by mechanical and dielectric analyses.

The strict additivity of the heat-capacity contributions of the group vibrations and the continuous

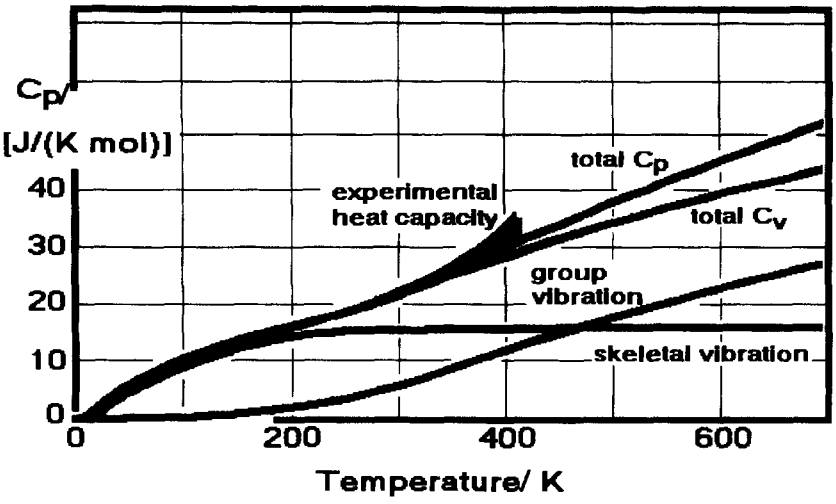

Fig. 8. Heat capacity of crystalline polyethylene.

change in Θ_1 with chemical composition led to the development of addition schemes for heat capacities. As long as the contributions of the backbone groupings that make up the polymer are known empirically, an estimate of the heat capacity of unknown polymers and copolymers is possible. Detailed tables can be found in [56,57].

The *heat capacities of liquids* are much more difficult to understand. The motion involves, besides the vibrations discussed in the last section, also large-amplitude rotations, internal rotations (conformational motion) and translations. Only a first beginning has been made in the more detailed discussion of the heat capacities of liquid macromolecules [48]. In the liquid state, polymers are usually at higher temperature and in thermodynamic equilibrium. It was discovered on hand of the large volume of data on liquid macromolecules that addition schemes can help to connect these heat capacities [56,57]. The experimental data for liquid, aliphatic polyoxides can be represented, for example, by the equation:

$$C_p^a = N_C[17.91 + 0.0411T] + N_O[28.13 - 0.0071t]\,J\,K^{-1}\,mol^{-1} \quad (14)$$

with N_C and N_O representing the number of C- and O-atoms in the repeating unit. Similar equations are available for nylons and polyesters [55]. The heat capacities of many macromolecules are thus available through measurement, computation from approximate vibration spectra, or empirical addition schemes.

Apparent heat capacities are heat-capacity-like effects measurable in regions where the analyzed samples are not in equilibrium or in a metastable state. Under such conditions, heat capacities appear time-dependent, and irreversible thermodynamics needs to be applied for the discussion of the data [9]. In all cases, large-amplitude motions are involved in such apparent heat capacities. With DSC, and even more so with the new TMDSC, the apparent heat capacities can be determined and used to study the kinetics and mechanisms of the irreversible processes. The glass-transition region offers apparent heat-capacity effects in the form of hysteresis phenomena and changes in the glass-transition temperature with time scale. The hysteresis of atactic polystyrene was discussed, in detail, based on dynamic differential thermal analysis data (DDTA) [58]. A first-order transition kinetics was used for the analysis, as is suitable for the basic irreversible thermodynamics [9], or a simple hole model of liquids.

The frequency dependence of the glass transition of amorphous poly(ethylene terephthalate) is shown in Fig. 9 based on TMDSC [60]. The ΔC_p represents the reversing heat capacity, as measured using Eq. (6) for quasi-isothermal measurements, i.e. each point is a separate experiment. Actual measurements were made with modulation periods in the (30–90) s. The other

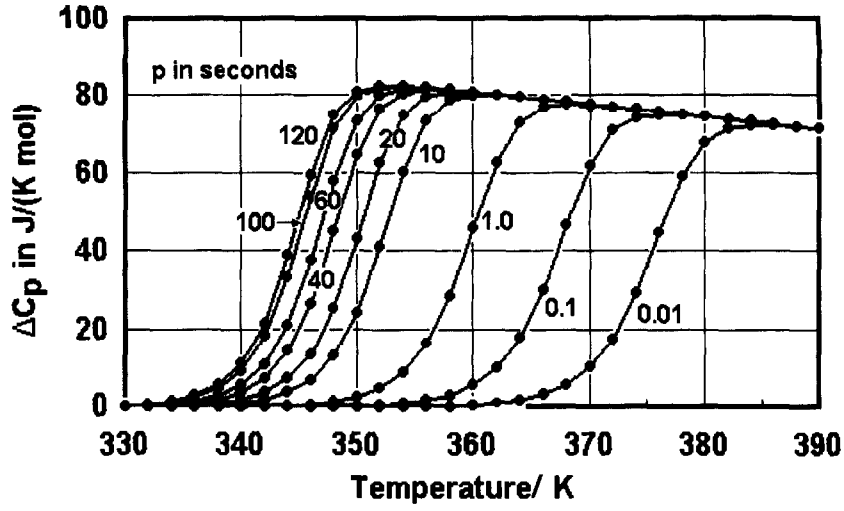

Fig. 9. Apparent increase in heat capacity of ply(ethylene terephthalate) when measured by TMDSC and extrapolated to modulation periods outside of the experimental range. Plotted is the averaged reversing heat capacity, eliminating second harmonic contributions [59].

points are extrapolated using the applied first-order kinetics. For the first time, it is now possible to directly compare thermal analysis to dynamic, mechanical and dielectric analyses [41].

The similarity of the description of temperature-modulated DSC and dynamic mechanical analysis (DMA) and also dielectric thermal analysis (DETA) has brought up the question whether a *complex heat capacity* (ratio: heat flow/temperature change) would be of use in analogy to the modulus in DMA (ratio: stress/strain). It was suggested that one could write for the complex heat capacity [61]:.

$$C^* \equiv C' - iC'' = C_0 e^{-i\theta} \tag{15}$$

where C' is the real part or the instantaneous response to a change in temperature (in analogy to the storage modulus of DMA), and C'' is the imaginary, delayed part (in analogy to the loss modulus of DMA). It follows, then, that the absolute amount of the heat capacity is:

$$|C_0| = \sqrt{(C')^2 + (C'')^2} \tag{16}$$

In analogy to the mechanical modulus, which is the ratio of peak stress to peak strain, C_0 is proportional to the ratio of peak-temperature-to-amplitude times frequency, i.e. it corresponds to the apparent heat capacity discussed in the prior paragraph.

In DMA experiments, G is the shear modulus, σ the stress, ε the strain, and θ the phase lag. In TMDSC, the heat flow, HF, corresponds to σ, and A to ε (see Eqs. (5) and (6)). The phase angle θ is determined relative to strain and sample temperature, respectively. To get a sample-specific complex heat capacity, it is necessary to make sure that steady state is maintained and negligible temperature gradients exist within the sample during the modulation cycles. In case of a sample that has no slowly responding modes of motion, as in the polymeric solids which have only vibrational motion, there should be no lag θ due to the sample response. The apparent heat capacity in the glass-transition region shown in Fig. 9, in contrast, is time-dependent and there should be a phase angle of the heat flow relative to the amplitude of the sample temperature caused by the sample response.

In a sample with a time-dependent, apparent heat capacity, one determines in some TMDSC (TA Instruments MDSC) the ratio of the maximum amplitude of $HF(t)$ to the maximum amplitude of the temperature at constant frequency (Eq. (6), i.e. the derived capacity is still C_0, the absolute amount of the heat capacity). This can now be separated into real and imaginary components with the sample-specific phase angle θ. The real part of the heat capacity accounts for a seeming

storage part, where heat is transferred in the given time interval, in-phase with the temperature change. The actual process is as follows: At a given time and corresponding temperature, heat flows into the sample to equilibrate temperature between sample and surroundings (ideally without temperature gradient, so that there is no change in entropy). Any slow kinetics, as for example in the glass-transition region, limits the heat transfer. If, after a given time interval, the sample could be kept adiabatically, the temperature would slowly decrease as the kinetics permits approach to internal equilibrium. As temperature and time change in the modulation experiment, the heat needed to reach internal equilibrium contributes to the heat flow at a higher temperature, accounting for the out-of-phase heat flow.

For a typical measurement through the glass transition, the phase lag is rather small (a few degrees). The real part of the heat capacity is linked to the part of the enthalpy gain of the sample that behaves as if the heat flow were instantaneous. The integral of this part of the complex heat capacity over one modulation period is obviously zero. The question remains what is this imaginary part? In the case of the complex mechanical modulus in a DMA experiment, this question is easy to answer. The complex modulus is linked to work done on, and recovered from the sample. By integration of the complex stress σ over the sinusoidal change in strain ϵ, one finds that the energy dissipated over one cycle, $\Delta W''$, is given by $-G''\varepsilon_0^2\pi$, while $\Delta W' = 0$. The analogous integral for heat dissipated over one modulation cycle would be: $\oint C_0 \sin(\omega t - \theta) \mathrm{d}(A \sin \omega t)$, and results in an enthalpy 'loss' of $-A\pi C'' = -A\pi C_0 \sin\theta$ from the out-of-phase part of the complex heat capacity, i.e. the imaginary part of the heat capacity violates the first law of thermodynamics, and therefore the integral is not a valid assessment of the enthalpy change. To check on the enthalpy balance, the heat flow, not the complex heat capacity, must be integrated over one period of time, only this gives the required conservation of energy. It is, however, easy to see that, since the imaginary part of the heat capacity is exchanged at a temperature different from the equilibrium, it must thus lead to an entropy production. Computing, then, over one cycle $\oint (C_0/T) \sin(\omega t - \theta) \mathrm{d}(A \sin \omega t)$, the in-phase part contributes, again as expected, zero, while the out-of-phase, imaginary part shows an entropy production of $AC''\pi/T_0$ (note that $T_0(1 + A \sin \omega t) \approx T_0$). The imaginary part of the complex heat capacity corresponds, thus, to an entropy loss that has occurred because the real heat capacity was supplemented by a change in enthalpy at a higher or lower temperature. While the loss modulus in DMA corresponds to a real loss (work to heat conversion), the entropy production does not (see Section 2).

Further discussion of this still controversial topic can be found in the proceedings of the Fourth Lähnwitz Seminar held in Krugsdorf, Germany, in June 1996 [62]. Also discussed at this seminar was the method of measuring complex heat capacity in the (0.2–2000) Hz frequency range using spectroscopy. A consistent picture has not yet been achieved, but the method which involves the determination of the third harmonic of heat dissipation of a heater imbedded in the sample, shows great promise.

7. Broad transitions

The final topic in this update on heat capacities of polymers is the occurrence of broad transitions during a heat-capacity measurement, a rather common occurrence. While a sharp glass transition or endotherm of a first-order transition can be easily recognized, broad transitions are more difficult to see. In addition, it may be possible that certain transitions expected from equilibrium considerations do not occur and the sample freezes on cooling to a disordered state. Such properties are common in conformationally disordered crystals [35].

Fig. 10 illustrates a rather *broad glass transition* in a poly(oxybenzoate-co-naphthoate) (58/42 mol%) [63]. The small endotherm (dotted area) indicates some additional minor entropy effects above the glass transition, involving mesophase transitions. Without an independent assessment of the solid and liquid heat capacities by measurement at lower and higher temperature and the evaluation of the vibration-only heat capacity, it would not have been possible to find the glass transition. The broad change of heat capacity in the transition region is a measure of the change in mechanical properties of this technologically important, modern polymer. Broad glass transitions are also common in partially crystalline and mesophase polymers, as well as in solutions of polymers [9]. In

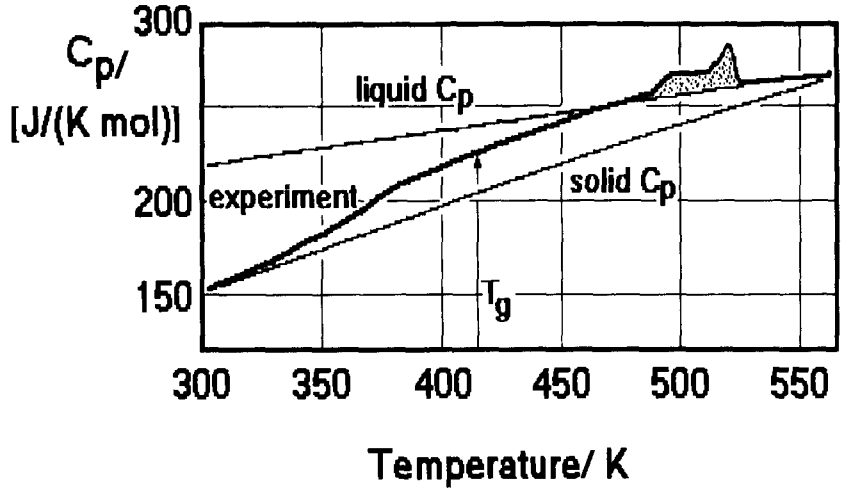

Fig. 10. Measured, and extrapolated heat capacities of poly(oxybenzoate-co-naphthoate) crystallized from the melt and measured by standard DSC on heating [63].

addition, one expects the decrease in phase sizes to micro- and nanophases to broaden transitions due to surface effects. The special changes of the equilibrium and apparent heat capacities in the glass-transition region of partially crystalline poly(ethylene terephthalate) are discussed in [64] on the basis of TMDSC.

A common effect in polymers is the shift of the upper end of the glass transition to higher temperatures on partial ordering, as already seen in Fig. 10. The main cause of this increase of the glass transition of a part of the material is introduced by strain into the amorphous phase by molecules crossing the phase boundary with a more ordered phase. In some cases, this strain is so large that a *rigid amorphous fraction* is produced. The rigid amorphous fraction decreases the heat capacity change at the glass-transition temperature, as illustrated in Fig. 11 for poly(oxymethylene) [65]. The shaded area is a measure of the decrease of the change of heat capacity with increasing crystallinity due to the rigid amorphous fraction which, in the case of poly(oxymethylene), does not become mobile until the crystals melt. Again, in order to properly assess the rigid amorphous fraction, both liquid and solid heat capacities must be available from measurements outside the transition region.

Broad melting transitions are very common in polymers [3]. Typical are melting ranges of (10–50) K as shown, for example, for poly(ethylene terephthalate) in Fig. 12 [66]. The standard DSC trace (upper left) shows, in addition, a broadened glass transition (compare with the amorphous sample seen in the upper right trace) and some rigid amorphous fraction. The heavy black line in the upper left figure is lower than expected for the heat capacity for a sample of the crystallinity measured from the heat of fusion (≈45%). To analyze the coupling of the broadening of the melting region and the rigid amorphous fraction, quasi-isothermal TMDSC measurement were made on the different sample of Fig. 12. The melt crystallized sample in the upper left shows little difference between DSC and TMDSC up to ≈450 K (except for the small time dependence of the heat capacity in the glass-transition region, see Fig. 10). More complicated is the assessment of the latent-heat producing process. It shows in its quasi-isothermal analysis that, even for polymers, a small amount of the melting is reversible, despite the fact that all flexible polymers have a (6–10) K metastability gap between melting and crystallization, i.e. either process should be nonreversing as long as the modulation amplitude is smaller than the metastability gap. The metastability gap was ascribed earlier to the lack of *molecular nucleation* in this temperature range [67–69]. Besides, from melting rate studies, this molecular nucleation could be documented by

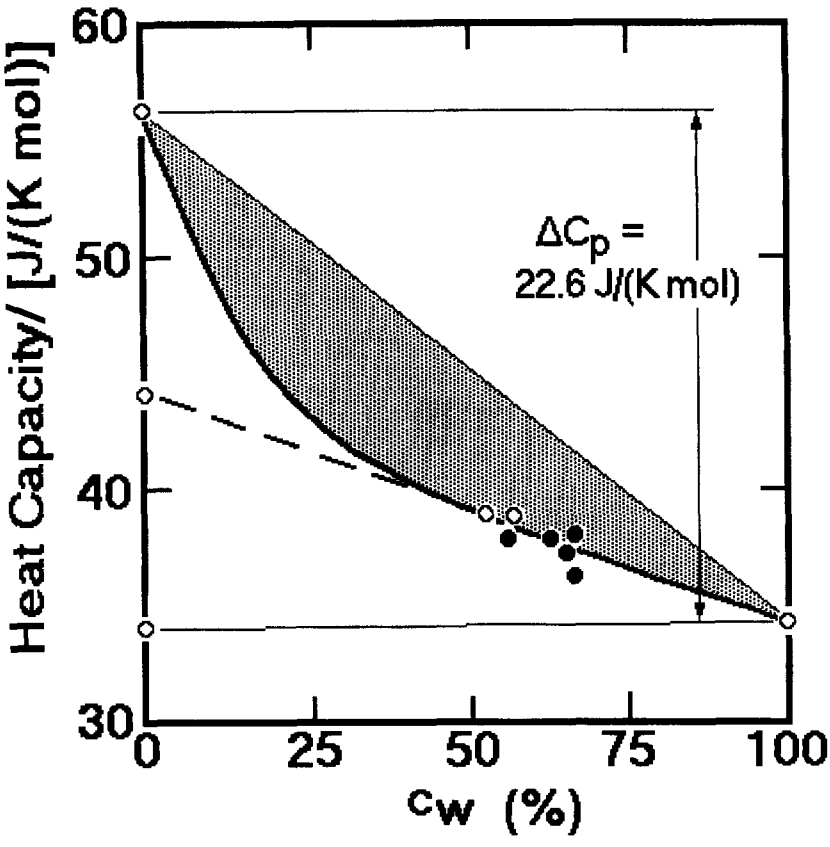

Fig. 11. Rigid amorphous fraction in poly(oxymethylene) as determined by a heat capacity vs. crystallinity (or heat of fusion) plot [65].

rejection of fractions of macromolecule from growing crystals of larger molar mass below their melting temperature, which proved the existence of a reversible process at this lower-than-equilibrium melting/crystallization temperature. This reversing process seems to be directly observable in the quasi-isothermal experiment of Fig. 12. Tedious experiments with DSC and dissolution could already show that, indeed, there was a small reversing fraction on dissolution that could not be extracted from the sample, i.e. it was still attached to the crystals [70]. It seems that TMDSC may permit a quantitative analysis of this reversible melting on a scale smaller than the macromolecule. Partially molten segments (in steady state) can recrystallize by minor reversal in temperature.

On the other three traces of Fig. 12, differently run samples are compared to the upper left TMDSC trace that is repeated in each graph with open circles. These graphs prove that the amount of polymer participating in the reversing melting is morphology and processing-dependent, and their analysis may be a valuable characterization tool. The melt-quenched sample in the upper right shows the glass transition, followed by crystallization at ≈370 K (not observable in reversing heat flow at steady state). The cold-crystallized sample has only a small increase in reversing fusion. On cooling from the melt, crystallization occurs only at ≈500 K (lower left in Fig. 12). It is interesting to note that the reversing melting remains closely similar to the original melt-crystallized sample. The lower right graph, finally, shows a drawn film. Here the glass transition is broadened considerably more, but the reversing melting fraction has not increased much. It is hoped that this new tool to analyze transitions will

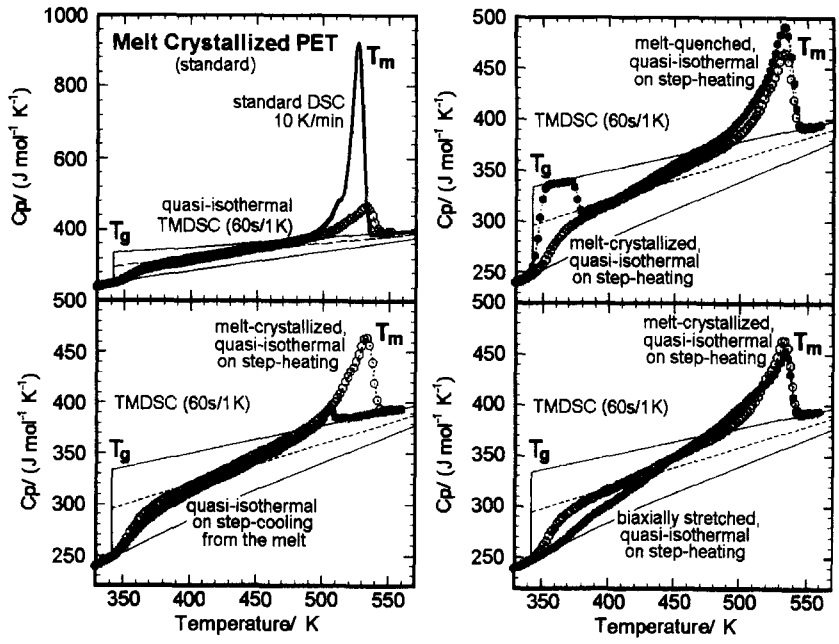

Fig. 12. Total heat capacity by standard DSC and reversing heat capacities by TMDSC for different samples of poly(ethylene terephthalate) [66].

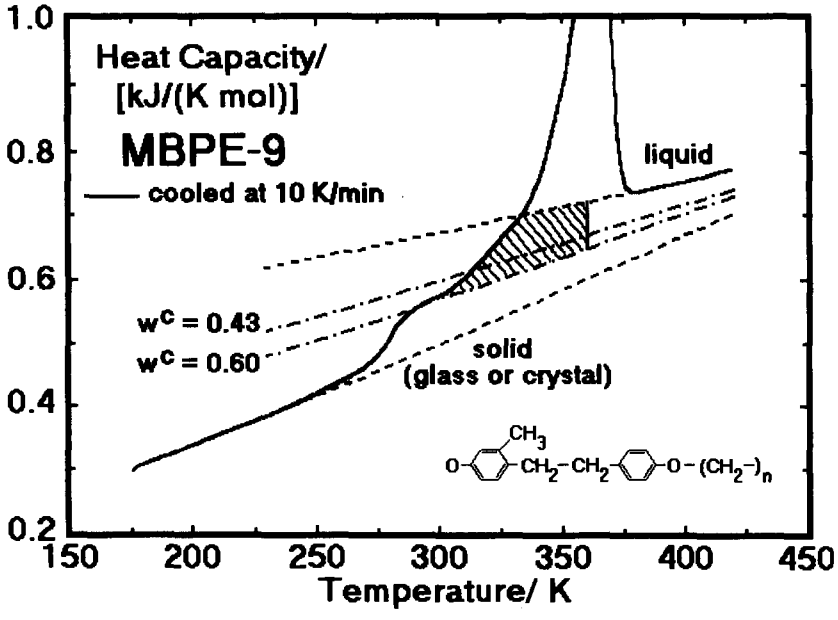

Fig. 13. Heat capacity of MBPE-9. The repeating unit formula is given in the figure [71].

lead when coupled with quantitative evaluation of heat capacity to a much more detailed description of the multiple nanophase structures of polymers.

A final example of a broad transition in a polymer is given in Fig. 13. It shows a standard DSC trace of a sample of poly[oxy(3-methyl-1,4-phenylene)ethylene-1,4-phenyleneoxynonamethylene], called for short MBPE-9, cooled from the melt [71]. Detailed structure (X-ray) and mobility studies (solid state NMR) could resolve many of the heat capacity, phase, and transition problems [71–73]. The low temperature heat capacity agrees, as expected, with a vibration-only solid. The glass transition is somewhat broadened toward lower temperature, as also observed for polyethylene (see Fig. 6). The crystals in this sample are conformationally disordered (see Fig. 4) and reach a crystallinity of 43%. From the liquid and solid heat capacities, one concludes that there is some rigid-amorphous fraction present (compare the two dash-dotted lines). The broad melting peak seems typical for polymers, but the heat capacity at the beginning of the melting peak is closer to the liquid than to the solid. Such high heat capacities are common in conformationally disordered crystals [35]. With this observation, one must assume that the enthalpy from the shaded area in Fig. 13 is not a latent heat of transition, but corresponds to a continuous decrease in entropy (increase in ordering, outside the transition region). This liquid-like heat capacity decreases continually when tracing Fig. 13 to lower temperature, indicating a broad glass transition of the mobile parts of the condis crystal. (Note that the low-temperature glass transition originates in the amorphous phase, not the condis crystals.) An overall accounting for the conformational entropy, as suggested in Fig. 4, is in agreement with this interpretation. Similar examples of continuous decrease in the conformational entropy of condis crystals and ultimate freezing, before full crystalline order has been reached, has been found by now for several large, as well as small molecules.

8. Conclusions

The heat capacity of polymers is an increasingly important part of sample characterization. Although thermal analysis was initially slow in finding the proper link to molecular motion, this is now well established and many effects not otherwise detectable can be analyzed. While the early work on heat capacity of polymers was mainly based on equilibrium considerations and often required extrapolation to not-actually-realizable states, the new developments in TMDSC indicate that it will be possible to follow the irreversible processes and study metastable polymers directly.

Acknowledgements

This work was supported by the Division of Materials Research, National Science Foundation, Polymers Program, Grant #DMR90-00520 and Oak Ridge National Laboratory, managed by Lockheed Martin Energy Research Corp. for the U.S. Department of Energy, under contract #DE-AC05-960R22464. Some support came also from TA Instruments Inc. and ICI Paints.

References

[1] H. Staudinger, Arbeitserinnerungen, Hüthing Verlag, Heidelberg, 1961.
[2] J. Dalton, A New System of Chemical Philosophy. London, 1808; the ideas appeared first in his notebook covering 1802–1804.
[3] B. Wunderlich, Macromolecular Physics, Vol. 3, Crystal Melting, Acdemic Press, New York, 1980.
[4] A. Lavoisier, Elements of Chemistry, Paris, 1789.
[5] B.G. Sumpter, D.W. Noid, G.L. Liang and B. Wunderlich, Atomistic dynamics of macromolecular crystals, Adv. Polymer Sci., 116 (1994) 27.
[6] A. Einstein, Ann. Physik, 22 (1907) 180, 800.
[7] P. Debye, Ann. Phys, 39 (1912) 789.
[8] W. Nernst, Ann. Physik, 36 (1911) 395.
[9] B. Wunderlich, Thermal Analysis, Academic Press, Boston, 1990.
[10] J.C. Southard and F.G. Brickwedde, J. Am. Chem. Soc., 55 (1933) 4378.
[11] A.E. Worthington, P.C. Marx and M. Dole, Rev. Sci. Instr., 26 (1955) 698.
[12] F.E. Karasz, H.E. Bair and J.M. O'Reilly, J. Phys. Chem., 69 (1965) 2657.
[13] F.S. Dainton, D.M. Evans, F.E. Hoare and T.P. Melia, Polymer, 3 (1962) 263, 271, 277, 286, 297, 310, 316, 317.

[14] B. Wunderlich and H. Baur, Adv. Polymer Sci., 7 (1970) 151.
[15] M. LeBlanc and M. Kröger, Z. Elektrochem., 34 (1928) 242.
[16] N. Bekkedahl and H. Matheson, J. Res. Natl. Bur. Stand., 15 (1935) 503.
[17] C.T. Anderson, J. Am. Chem. Soc., 59 (1937) 1036.
[18] F.T. Gucker Jr.W.L. Ford, J. Am Chem. Soc,., 60 (1938) 2563.
[19] V.V. Tarasov, Zh. Fiz. Khim., 24 (1950) 111.
[20] W.H. Stockmayer and C.E. Hecht, J. Chem. Phys., 21 (1953) 1954.
[21] B. Wunderlich, J. Thermal Analysis, 46 (1966) 643.
[22] B. Wunderlich, Macromolecular Physics, Vol. 1, Crystal Structure, Morphology, Defects, Vol. 2, Crystal Nucleation, Growth, Annealing, Academic Press, New York, 1974, 1976.
[23] B. Wunderlich, Macromolecular Chem. Phys., to be published.
[24] B. Wunderlinch and J. Grebowicz, Adv. Polymer Sci, 60/61 (1984) 1.
[25] B. Wunderlich, The ATHAS data base on heat capacities of polymers, Pure Applied Chem., 67 (1995) 1919.
[26] U. Gaur, H.-C. Shu, A. Mehta, S.-F. Lau, B.B. Wunderlich, M. Varma-Nair and B. Wunderlich, J. Phys. Chem. Ref. Data, 10 (1981) 89, 119, 1001, 1051; 11 (1982) 313, 1065; 12 (1983) 29, 65, and 20 (1991) 349.
[27] B. Wunderlich, J. Phys. Chem., 64 (1960) 1052.
[28] P. Ehrenfest, Acad. Sci., Amsterdam, Suppl. 75b Mitt. Kammerlingh Onnes Inst., Leiden, 36 (1933) 153.
[29] J.W. Richards, Chem. News, 75 (1897) 278.
[30] P. Walden, Z. Electrochem., 14 (1908) 713.
[31] H. Kelker, History of liquid crystals, Mol. Cryst. Liq. Cryst., 21 (1973) 1.
[32] G.W. Gray, Molecular Structure and the Properties of Liquid Crystals, Academic Press, New York, NY, 1962.
[33] G.W. Gray and P.A. Winsor, Eds., Liquid Crystals and Plastic Crystals. Wiley, Chichester, England, 1974, Vol. 1.
[34] G.W. Smith, in: G.H. Brown (Ed.), Advances in Liquid Crystals, Academic Press, New York, NY, 1975, Vol. 1; p. 193.
[35] B. Wunderlich, M. Möller, J Grebowicz and H. Baur, Conformational Motion and Disorder in Low and High Molecular Mass Crystals, Adv. Polymer Sci., Vol. 87, Springer Verlag, Berlin, 1988.
[36] F.H. Müller and H. Martin, Kolloid Z., 172 (1960) 97; M.J.O' Neill, Anal. Chem., 36 (1964) 1238.
[37] A. Boller, Y. Jin and B. Wunderlich, J. Thermal Anal., 42 (1994) 307.
[38] M. Reading, D. Elliot and V.L. Hill, J. Thermal Anal., 40 (1993) 949; P.S. Gill, S.R.Sauerbrunn and M. Reading, J. Thermal Anal., 40 (1993) 931; M. Reading, Trends in Polymer Sci., 8 (1993) 248.
[39] B. Wunderlich, Y. Jin and A. Boller, Thermochim. Acta, 238 (1994) 277.
[40] B. Wunderlich, A. Boller, I. Okazaki and S. Kreitmeier, Thermochim. Acta, 282/283 (1996) 143.
[41] A. Boller, C. Schick and B. Wunderlich, Thermochim. Acta, 266 (1995) 97.
[42] B. Wunderlich and A. Boller, in Shaheer A. Mikhail (Ed.), Proc. 24th NATAS Conf., San Francisco, CA, Sept. 10–13, 1995, pp. 136–141; Full version by A. Boller, I. Okazaki, and B. Wunderlich, Thermochim. Acta, 284 (1996).
[43] B. Wunderlich, Pure and Applied Chem., 67 (1995) 1919.
[44] M. Born and T. V. Kármán, Phys. Z., 13 (1912) 297; 14 (1915) 15.
[45] B. Wunderlich, J. Chem. Phys., 37 (1962) 1203, 1207.
[46] For computer programs and general discussion of the Debye functions, see Yu. V. Cheban, S.F. Lau and B. Wunderlich, Coloid Polymer Sci., 260 (1982) 9.
[47] B. Wunderlich, J. Chem. Phys., 37 (1962) 2429.
[48] K. Loufakis and B. Wunderlich, J. Phys. Chem., 92 (1988) 4205.
[49] J. Barnes and B. Fanconi, J. Phys. Chem. Ref. Data, 7 (1978) 309.
[50] H.S. Bu, S.Z.D. Cheng and B. Wunderlich, J. Phys. Chem., 91 (1987) 4179.
[51] R. Pan, M. Varma and B. Wunderlich, J. Thermal Anal., 35 (1989).
[52] J. Grebowicz, H. Suzuki and B. Wunderlich, Polymer, 26 (1985) 561.
[53] G. Zhang and B. Wunderlich, J. Thermal Anal., 47 (1996) 899.
[54] D.W. Noid, M. Varma-Nair, B. Wunderlich and J.A. Darsey, J. Thermal Anal., 37 (1991) 2295.
[55] Check our home page on the WWW: http://funnelweb.utc-//funnelweb.utcc.utk.edu/~athas.
[56] U. Gaur, M.-Y. Cao, R. Pan and B. Wunderlich, J. Thermal Anal., 31 (1986) 421.
[57] R. Pan, M.-Y. Cao and B. Wunderlich, J. Thermal Anal., 31 (1986) 1319.
[58] B. Wunderlich, D.M. Bodily and M.H. Kaplan, J. Appl. Phys., 35 (1964) 95.
[59] B. Wunderlich and I. Okazaki, J. Thermal Anal., 49 (1997).
[60] B. Wunderlich and I. Okazaki, PMSE Proceedings, 76 (1997) 217.
[61] J.E.K. Schawe, Thermochim. Acta, 261 (1995) 183.
[62] Proceedings, to be published in a special issue of Thermochim. Acta in 1997.
[63] M.-Y. Cao, M. Varma-Nair and B. Wunderlich, Polymers for Advanced Technology, 1 (1990) 151.
[64] I. Okazaki and B. Wunderlich, J. Polymer Sci., Part B: Polymer Phys., 34 (1996) 2941.
[65] H. Suzuki, J. Grebowicz and B. Wunderlich, British Polymer J., 17 (1985) 1.
[66] I. Okazaki and B. Wunderlich, Macromolecules, 30 (1997) 1758.
[67] B. Wunderlich, Disc. Farad. Soc., 68 (1979) 239.
[68] B. Wunderlich and A. Mehta, J. Polymer Sci., Polymer Phys. Ed., 12 (1974) 255.
[69] A. Mehta and B. Wunderlich, Colloid and Polymer Sci., 253 (1975) 193.

[70] A. Mehta and B. Wunderlich, Makromolekulare Chemie, 175 (1974) 977.
[71] Y. Jin, J. Cheng, B. Wunderlich, S.Z.D. Cheng and M.A. Yandrasits, Polymers for Advanced Technology, 5 (1994) 758.
[72] J. Cheng, Y. Jin, B. Wunderlich, S.Z.D. Cheng, M.A. Yandrasits, A. Zhang and V. Percec, Macromolecules, 25 (1992) 5991.
[73] M.A. Yandrasits, S.Z.D. Cheng, A. Zhang, J. Cheng, B. Wunderlich and V. Percec, Macromolecules, 25 (1992) 2112.